LARS Information Note 042473

Geometric Aspects in Digital Analysis of Multi-spectral Scanner (MSS) Data

by
E. M. Mikhail
J. R. Baker

The Laboratory for Applications of Remote Sensing
Purdue University, West Lafayette, Indiana
1973

GEOMETRIC ASPECTS IN DIGITAL ANALYSIS OF MULTI-SPECTRAL SCANNER (MSS) DATA*

Edward M. Mikhail and James R. Baker
School of Civil Engineering
Purdue University
West Lafayette, Indiana 47907

BIOGRAPHICAL SKETCHES

Edward M. Mikhail, BS (Honors), Cairo University, MS and PhD, Cornell University, Winner of two research photogrammetric awards. Two years with private industry as research analytical photogrammetrist. Member of the Faculty of Purdue University, since 1965, in charge of graduate instruction and research in photogrammetry, adjustment, and hologrammetry. Consultant to industry, and government particularly U.S. Army Mapping organizations. Published numerous technical papers and reports. Recepient to a NATO postodoctoral fellowship in 1971 for one-year sabbatical in Europe, where he did research on adjustment and remote sensing, and lectured on hologrammetry.

James R. Baker is currently graduate instructor at Purdue University where he is performing research in remote sensing in conjunction with the Laboratory for Applications of Remote Sensing (LARS); B.S.C.E. and M.S. degrees from the University of New Mexico, and an M.S.C.E. degree from Purdue University. Currently a PhD candidate at Purdue. Assistant Professor of Engineering at Fort Lewis College for four years, when he received an NSF Science Faculty Fellowship to attend Purdue. Winner of numerous academic honors, including the Cubic and Kueffel and Esser fellowships of the American Congress on Surveying and Mapping (ACSM).

ABSTRACT

Present automated systems of interpretation which apply pattern recognition techniques on MSS data do not fully consider the geometry of the acquisition system. Metric information cannot therefore be extracted from the data at the same time that interpretation is performed. In an effort to improve the usefulness of the MSS data when digitally treated, geometric aspects are analyzed and discussed. Attempts to correct for scanner instabilities in position and orientation by affine and polynomial transformations, as well as by modified collinearity equations are described. Methods of accounting for panoramic and relief effects are also discussed. It is anticipated that reliable area as well as position determinations can be accomplished during the process of automatic interpretation. The paper is concluded by presenting a concept for a unified approach to the treatment of remote sensing data, both metric and non-metric.

---

*This paper was presented at the Spring Convention of the American Society of Photogrammetry, Washington, D.C. March 7-11, 1973. This work was supported in part under NASA Grant Number NGL 15 - 005 - 112.

INTRODUCTION

Remote sensing is an all inclusive term used to describe information recording about objects and phenomena without physical contact, and the analysis of the recorded information. Therefore, conventional activities of photogrammetry and photointerpretation fall within the realm of remote sensing.

There are many remote sensing systems which may be classified according to different criteria: (1) whether stationary or on a moving platform, (2) whether image-forming or not, (3)whether passive or active, and (4) according to the geometric characteristics of the information gathered (i.e., positional, directional, distance, etc.). When one is concerned with information regarding the Earth and its environment, sensors on moving platforms, from the air, space, or water, are usually used. Furthermore, since many of the techniques of evaluation are adapted from photogrammetric and interpretive techniques developed in the past, interest focuses on remote systems with potential image-forming capability.

The active-passive classification depends upon whether the sensor generates its own source of energy or not. Passive systems are those responding to energy reflected or re-emitted from the object space and include: cameras such as frame, panoramic, or continuous strip; optical-mechanical scanners such as the infrared line scan (IRLS), multi-spectral scanner (MSS), etc.; and radiometers, such as conical, zig zag, etc. Active image-forming systems generate their own signals, such as radar (rotating PPI, side-looking SLAR with realor synthetic aperture), or sonar.

Classification as regards geometry would include area recording (e.g., frame camera), line recording (e.g., panoramic and continuous strip cameras), or point recording (e.g., optical mechanical scanners and scanning radiometers). The information may be related to position, or to distance by echo-time as in radar.

This brief review, then, indicates that the system of interest in this paper, the MSS, is a passive system used on a moving platform, both aircraft and spacecraft, with potential image formation, and records object data in a point by point mode. The term "point" is used here to mean a small, though finite, area representing the system's resolution element as will be explained in detail later on.

The potential of MSS, and of remote sensors in general, is becoming more apparent as man attempts to cope with a variety of problems from resources mapping to environmental monitoring. These systems are utilized aboard aircraft, as well as spacecraft such as the present ERTS, and planned Skylab. In order to appreciate the nature and amount of data acquired by the MSS system a brief description of its basic concept is given.

The MSS system

In simplified terms, the multispectral scanner contains a rotating prism which scans the terrain in narrow strips or lines oriented normal to the direction of flight. The forward motion of the aircraft provides continuous coverage by allowing some overlap between successive strips. The incoming energy reflected off the rotating prism is divided into several wavelength bands, each band recorded separately (figure 1a).

At any instant of time, energy from a finite object area $(\Delta x)(\Delta y)$, see figure 1b, determined by the angular resolution of the system, is represented by a set of numbers, one for each band. In each band, the number for one resolution element represents the spectral radiance from that area on the terrain. A fixed number of consecutive resolution elements side by side form a scan line. The data is usually recorded on magnetic tape, which after pre-processing yields the information in digital form. For each resolution element, there is a position in a matrix representing the scan line number in one dimension, and the element number within that line, in the other dimension. Associated with that position would be several spectral values equal in number to the spectral bands of the system.

Data in this format is so extensive that only automated digital techniques would be practical for its processing. One such digital system, which relies on pattern recognition and statistical classification algorithms, has been developed at the Laboratory for Applications of Remote Sensing (LARS) of Purdue University. This system makes possible efficient analysis, interpretation, and classification of such digital data automatically.

Extensive digital algorithms for automatic interpretation have by necessity disregarded or subordinated the geometrical aspects of the acquisition system. These algorithms relied extensively on strictly statistical techniques. To the photogrammetrist, however, such approach may be unnecessary since functional models can be constructed and utilized, perhaps with simplifications, without resorting to stochastical methods. Recognition of the geometric elements of the system, and proper account for them, would improve the interpretive results, as well as provide further useful quantitiative information from the data.

THE REMOTE SENSING TRANSFORMATION FOR MSS

Remote sensing can be thought of as a mapping of a multi-dimensional space onto another space with the same or fewer dimensions. This mapping may be considered in a general sense to be effected through a transformation taking a multidimensional vector into another multidimensional vector. We shall call this the remote sensing transformation, which transforms an object space vector into a sensor space vector. The dimensions of each vector will depend upon the degree of simpliciation of the physical phenomena involved, and the characteristics of the sensor to be employed.

Treated generally, the concept of remote sensing as a transformation is a broad approach intended to amalgamate two classically separated activities: the interpretive and the quantitative. It attempts to unify both the metric and non-metric aspects of remote sensing. Therefore, the elements of the vectors involved may include geometric, dynamic, and energy components, with corresponding broadening of the transformation parts. This unified approach is considered beyond the scope of this specific discussion, although further comments will be presented at the end of this paper.

Restricting the discussion to the MSS system, it is useful to note that passive optical-mechanical scanners can operate in several modes:

(a) Scanning in a plane normal to the flight direction

(b) Scanning in a plane oblique to the flight direction rotated about a horizontal axis normal to flight direction

(c) Hyperbolic Scan, or scanning in a cone with the flight direction as an axis

(d) Circular scan, or scanning in a cone with a vertical axis

The system with which this presentation is concerned is that in (a), because it is at present the more common, although the other three systems are available and may gain favor of use in the future. (The circular scan of (d) above is planned for skylab.)

To facilitate the understanding of the development to follow, we shall divide the sensing transformation into two parts: one concerned with geometric and time factors, and the other with energy aspects. We shall further concentrate on the first type of transformation since it composes the main theme of this paper.

In order to construct the sensor transformation, it is perhaps easier if one visualizes that the data from MSS forms an image instead of an array of numbers, one picture element or "pixel" for every spectral value number. The two dimensions of the matrix of numbers would be then equivalent to the size of the plane of imagery. Since each pixel, or spectral number, is recorded at a particular instant of time, then time as a variable (or element of both the object space and sensor space vectors) plays an important role. Therefore, let the following be the basic variables:

T_o the epoch or time of beginning of recording (at zero x-coordinate)

t_r time period for one revolution of the scanner

T_{ij} time of recording point j on scan line i

θ_{ij} instantaneous scan angle when point j is recorded (see figure 1b)

2α total scan angle (α on either side of plumb line)

c constant representing a "principal distance", or the equivalent of the radius of the cylindrical recording drum

v speed representing "film" advance when pictorial recording, or its equivalent when recording in other modes (magnetic tape, etc.), taken as a constant

$(x,y)_{ij}$ cartesian coordinates of point P_{ij} (either image or its equivalent in digital recording), see figure 2

y'_{ij} distance along scan line i between x-axis and P_{ij}

$\underline{A}_{ij}(t)$ instantaneous orientation matrix at T_{ij} (taking object system to sensor system)

k'_{ij}, k_{ij} scale factors between object and sensor spaces for point j on scan line i, ($k_{ij} = k'_{ij}/\cos\theta$)

$(X_c, Y_c, Z_c)_{ij}$ instantaneous position of exposure station at T_{ij}

$(X,Y,Z)_j$ object coordinates of any point

With the above variables, the following general relations may be written directly:

$$T_{ij} = T_o + it_r + \left(\frac{\alpha - \theta_{ij}}{2\pi}\right) t_r \qquad (1)$$

where i is the scan line number on which P_{ij} lies

$$x_{ij} = v\left[it_r + \left(\frac{\alpha - \theta_{ij}}{2\pi}\right) t_r\right] = v(T_{ij} - T_o) \qquad (2)$$

$$y'_{ij} = c\,\theta_{ij} \qquad (3)$$

$$y^2_{ij} = y'^2_{ij} - \left(\frac{v\,\theta_{ij}\,t_r}{2\pi}\right)^2 \qquad (4)$$

$$\frac{1}{k'_{ij}}\begin{bmatrix}1 & 0 & 0\\ 0 & \cos\theta_{ij} & -\sin\theta_{ij}\\ 0 & \sin\theta_{ij} & \cos\theta_{ij}\end{bmatrix}\begin{bmatrix}0\\0\\-c\end{bmatrix} = \underline{A}_{ij}(t)\begin{bmatrix}X_j-X_{cij}\\ Y_j-Y_{cij}\\ Z_j-Z_{cij}\end{bmatrix} \qquad (5)$$

On the basis of (2), (3), and (5) the four-dimensional sensor transformation becomes

$$\begin{bmatrix} x_{ij}\\ 0\\ \frac{c}{k_{ij}}\tan\left(\frac{y'_{ij}}{c}\right)\\ -\frac{c}{k_{ij}}\end{bmatrix}_{4,1} = \begin{bmatrix} v & \underline{0}\\ \underline{0} & \underline{A}_{ij}(t)\end{bmatrix}_{3,3}\begin{bmatrix} T_{ij}-T_o\\ X_j-X_{cij}\\ Y_j-Y_{cij}\\ Z_j-Z_{cij}\end{bmatrix}_{4,1} \qquad (6)$$

Equation (6) represents a rather general transformation for MSS when the scanning is performed in a plane normal to the direction of flight. For other modes of scanning, similar transformations can be derived.

In order to incorporate metric aspects into an extensive program for automatic interpretation, it is more practical to begin with a much simplified case, and progressively proceed toward the general situation given above. This is the way the research, on which this paper reports, actually proceeded.

ASSUMED IDEAL GEOMETRY

The simplest case is to assume ideal flight conditions, thus $\underline{A}(t) = \underline{I}$, and Z_c = constant above datum. This idealized situation is depicted in figure 3, in which $(X,Y,Z)_j$ are the object coordinates of any point J. Other parameters include: the angular resolution γ, aircraft velocity V, and an overlap factor of adjacent scan lines, S. With the orientation matrix being identity, equation (6) yields

$$X_j = X_{cj} \qquad (7)$$

If X_{co} is the X-coordinate of the exposure station at beginning of recording, then X_{ci} may be given by

$$X_j = X_{cj} = X_{co} + \int_o^{T_j} V\,dt \qquad (8)$$

where T_j is the time at the recording of point J. If we assume the overlap factor S is maintained constant, then from figure 3a one may write

$$(1-S)dX = Vdt \tag{9}$$

Since S is defined at the datum, then the left hand side may be written in terms of the sensor space as

$$(1-S)dX = (1-S)\frac{Z_c}{c}dx \tag{10}$$

and equation (8) becomes

$$X_j = X_{cj} = X_{co} + \int_0^{x_j} (1-S)\frac{Z_c}{c}dx \tag{11}$$

where x_j is the image x-coordinate of point J. Note that at the epoch, x = o, hence T_o is assumed to be zero, for simplicity. Equations (8) and (11) are general expressions for computing the X-coordinate of any point J under the above-stated assumptions. If in addition to Z_c, S is also assumed constant (i.e. independent of x, or consequently of time) equation (11) simplifies to

$$X_j = X_{cj} = X_{co} + \frac{Z_c(1-S)x_j}{c} \tag{12}$$

If we assume further that the scan rate is so fast that each scan line is considered recorded instantaneously, then y' becomes equal to y.

The Y-coordinate may be obtained from (6) directly, since with $\underline{A} = \underline{I}$,

$$\frac{c}{k_j}\tan\left(\frac{y_j}{c}\right) = Y_j - Y_{cj}$$

$$-\frac{c}{k_j} = Z_j - Z_c$$

or

$$Y_j = Y_{cj} + (Z_c - Z_j)\tan\left(\frac{y_j}{c}\right) \tag{13}$$

EFFECTS OF SCAN, TOPOGRAPHY, AND SENSOR EXTERIOR ORIENTATION

The idealized geometry assumed in the preceding section is obviously not realized in practice. There are several factors which occur and which affect the coordinates as derived by equations (12) and (13). Although if equation (6) is used directly these factors would be directly accounted for, we shall treat each separately in order to gain insight into the system.

(1) As shown in figure 3b, recording is done on a cylindrical, instead of a plane surface. This causes a panoramic appearance, which will be termed "scan angle effect".

(2) Removing the assumption that the object is a plane, leads to assigning elevations to different resolution elements. This will be called "topographic effect".

(3) Relaxing the assumption of ideal flight conditions leads to "sensor exterior orientation effects".

(4) When the assumption that each scan line is instantaneously recorded is not adhered to, then the effect of a finite time of scan will be designated "scan time effect".

Each of the above four effects will be addressed separately.

Scan angle effect

Figure 3b shows that A' is the position of point J on a plane, while A is the point actually recorded. The difference is

$$dy = OA' - OA = c(\tan \theta_j - \theta_j) \tag{14}$$

which represents the displacement due to scan angle effect. Note that

$\theta_j = \frac{y_j}{c}$, as was used in equation (13). (See also equation (3)). Within each scan line, the resolution element on the ground changes due to the same effect. The coverage of the scan line on the ground accordingly takes the shape of a "bow tie", and the effect is therefore often referred to by that name. From figure 1b, one may directly write:

$$\Delta X = \gamma (Z_c - Z) \sec \theta \tag{15}$$

$$\Delta Y = \gamma (Z_c - Z) \sec^2 \theta \tag{16}$$

If one approximates the area of ground resolution element ΔA by the product of ΔX and ΔY, then

$$\Delta A = \gamma^2 (Z_c - Z)^2 \sec^3 \theta \tag{17}$$

which implies a considerable variation of ΔA with the scan angle. As an example, if $(Z_c - Z) = 5000$ ft., $\gamma = 3$ mrad, then $\Delta A = 15' \times 15'$ at nadir, and $\Delta A = (\Delta X)(\Delta Y) = 19.5' \times 25.5'$ at $\theta = 40^o$.

To illustrate the change in the dimension of the resolution element in the scan direction, ΔY, figure 4 shows several plots. It depicts the variation in ΔY as a percentage of flying height above terrain $(Z_c - Z)$, due to change in scan angle θ, for a number of values of the angular resolution γ.

Topographic effect

Current interpretive systems assume flat terrain. This simplification can lead to serious planimetric displacement, as displayed in figure 5, given by

$$\delta Y = \delta Z \tan\theta \qquad (18)$$

In equation (18), δZ may represent total elevation if topographic effects have been totally neglected, or it may represent some height error, if some effort in assigning elevations to scan elements has been attempted. It is clear that $\delta Y = 0$ at nadir, $\delta Y = \delta Z$ at $\theta = 45^o$, and δY would increase rather rapidly as θ increases beyond 45^o.

Sensor exterior orientation effect

Equation (6) shows that both position and orientation of the sensor are functions of time, and therefore the assumption of ideal flight conditions is not realistic. The variations in elements of sensor exterior orientation are in general random, but the cumulative effect of these variations may be deterministic. (4) This led several investigators (4,8,9) to model the behaviour of these elements using such functions as polynomials and harmonics.

Ideally, the mathematical functions expressing the behaviour of exterior orientation elements should be in terms of time. However, time may not be recorded with sufficient accuracy to be relied upon for such analysis. Instead, if we utilize the concept of, v, as a constant effective speed of "film" travel, as mentioned previously, then the x-coordinate of the "imagery" may replace time in these functions. When the data recording is in the form of digital arrays, x may further be replaced by the scan line number i as the independent variable.

Thus, if Y_c is assumed to vary as a second order polynomial in time

$$Y_c = a_o' + a_1' t + a_2' t^2 \qquad (19)$$

then from (2), with T_o assumed zero, t may be replaced by x/v leading to

$$Y_c = a_o + a_1 x + a_2 x^2 \qquad (20)$$

where $a_o = a'_o \qquad a_1 = a'_1/v \qquad a_2 = a'_2/v^2$ (21)

The effect of variations in the orientation elements can be derived directly from equation (6). If we use θ for y/c and h for c/k, the 3-dimensional geometric portion of the transformation in (6), when inverted, becomes

$$\begin{bmatrix} X - X_c \\ Y - Y_c \\ Z - Z_c \end{bmatrix} = \underline{A}^t \begin{bmatrix} 0 \\ h \tan\theta \\ -h \end{bmatrix} \tag{22}$$

Starting with the case of $\underline{A} = \underline{I}$, we study the effect of small angles $d\omega$, $d\phi$, $d\kappa$ on the coordinates X,Y of an object point. Under $\underline{A} = \underline{I}$, equations (7) and (13) give the X, Y coordinates of the point, remembering that here

$$h = Z_c - Z .$$

It can be readily shown that

$$\frac{\partial \underline{A}}{\partial \omega} = \underline{A} \begin{bmatrix} 0 & 0 & 0 \\ 0 & 0 & 1 \\ 0 & -1 & 0 \end{bmatrix}; \quad \frac{\partial \underline{A}}{\partial \phi} = \underline{A} \begin{bmatrix} 0 & \sin\omega & -\cos\omega \\ -\sin\omega & 0 & 0 \\ \cos\omega & 0 & 0 \end{bmatrix}$$

$$\frac{\partial \underline{A}}{\partial \kappa} = \begin{bmatrix} 0 & 1 & 0 \\ -1 & 0 & 0 \\ 0 & 0 & 0 \end{bmatrix} \underline{A}$$

which under the assumptions of initial $\underline{A} = \underline{I}$ and small angles become

$$\frac{\partial \underline{A}}{\partial \omega} = \begin{bmatrix} 0 & 0 & 0 \\ 0 & 0 & 1 \\ 0 & -1 & 0 \end{bmatrix}; \quad \frac{\partial \underline{A}}{\partial \phi} = \begin{bmatrix} 0 & d\omega & -1 \\ -d\omega & 0 & 0 \\ 1 & 0 & 0 \end{bmatrix}; \quad \frac{\partial \underline{A}}{\partial \kappa} = \begin{bmatrix} 0 & 1 & 0 \\ -1 & 0 & 0 \\ 0 & 0 & 0 \end{bmatrix} \tag{24}$$

Equation (22) may now be differentiated to obtain the effects of angular and positional changes in the exterior elements. Note that differentiation with respect to h must also be performed since in it is contained the scale factor k which is a variable for each point.

$$\begin{bmatrix} dX - dX_c \\ dY - dY_c \\ dZ - dZ_c \end{bmatrix} = \begin{bmatrix} 0 & 0 & 0 \\ 0 & 0 & -1 \\ 0 & 1 & 0 \end{bmatrix} \begin{bmatrix} 0 \\ h \tan\theta \\ -h \end{bmatrix} (d\omega) + \begin{bmatrix} 0 & -d\omega & 1 \\ d\omega & 0 & 0 \\ -1 & 0 & 0 \end{bmatrix}$$

$$\begin{bmatrix} 0 \\ h \tan\theta \\ -h \end{bmatrix} (d\phi) + \begin{bmatrix} 0 & -1 & 0 \\ 1 & 0 & 0 \\ 0 & 0 & 0 \end{bmatrix} \begin{bmatrix} 0 \\ h \tan\theta \\ -h \end{bmatrix} (d\kappa) + \begin{bmatrix} 0 \\ dh \tan\theta \\ -dh \end{bmatrix} \tag{25}$$

It is important to point out that equation (22) is a projection from sensor space (which is essentially two-dimensional) to three-dimensional object space. Therefore it is not possible from single imagery to determine all three coordinates (X, Y, Z), because another unknown scale factor k is implicit in h. Therefore, as has been the practice in deriving differential formulas, we assume Z constant. Consequently, from the third equation in (25), enforcing d Z = 0, one gets

$$- dZ_c = h \tan\theta \; d\omega - dh$$

from which

$$dh = dZ_c + h \tan\theta \; d\omega \qquad (26)$$

Using (26) in the upper two equations of (25) and neglecting terms of second order gives:

$$dX = dX_c - h \, d\phi - h \tan\theta \; d\kappa \qquad (27a)$$

$$dY = dY_c + \tan\theta \; d Z_c + h \sec^2\theta \; d\omega \qquad (27b)$$

If we assume that Z_c is also a constant, h will be a constant and the equations in (27) may be added to equations (7) and (13) to yield

$$X = X_c + dX_c - h \, d\phi - h \tan\theta \; d\kappa \qquad (28a)$$

$$Y = Y_c + dY_c + h \tan\theta + \tan\theta \; dZ_c + h \sec^2\theta \; d\omega \qquad (28b)$$

The equations in (28) are the final form for evaluating the planimetric coordinates of an object point. Series expansion of $(\tan\theta)$, substituting back y/c for θ, and selecting appropriate polynomials for the exterior orientation elements, X_c, Y_c (note that dX_c, dY_c would be absorbed into the constant terms of the polynomials), $d\omega$, $d\phi$, $d\kappa$, would lead to the final polynomial expressions. These may be used in a usual interpolation operation using least squares if redundant horizontal control is available.

As an example, taking the first two terms in the expansion of $\tan\theta$ $(\tan\theta \cong \theta + \frac{1}{3}\theta^3)$, and using $(\tan^2\theta + 1) = \sec^2\theta$, and linear polynomials in x for the exterior orientation elements, leads to:

$$X = A_o + A_1 x + A_2 y + A_3 xy + A_4 y^3 + A_5 xy^3 \qquad (29)$$

$$Y = B_o + B_1 x + B_2 y + B_3 xy + B_4 y^3 + B_5 xy^3 + B_6 y^2 + B_7 xy^2 + B_8 y^4 + B_9 xy^4 + B_{10} y^6 + B_{11} xy^6 \qquad (30)$$

In some systems, the angle ω may be stabilized to less than one resolution element and therefore the last term in equation (28b), and correspondingly the six terms on the second line of equation 30 may be dropped.

Once the polynomial coefficients are determined, point-by-point numerical rectification may be performed using the same polynomials. There are other procedures of interpolation which may be used in conjunction with remote sensing data (11), such as linear least squares interpolation (10).

Scan time effect

If the assumption that each scan line is recorded instantaneously is relaxed, then the way data are recorded would be as shown in figure 2, a segment of which is enlarged in figure 6. The X coordinate of any point may be written as

$$X = X_c + \frac{Y'}{2\pi c} t_r V \tag{31}$$

where X_c corresponds to the central point (the nadir, under ideal flight conditions), V the aircraft velocity, and the other symbols as defined before. The effect shown by equation (31) can be incorporated with the others given in the preceding section, and polynomials used for the combined effects.

If the time period for one revolution t_r is not known sufficiently then, the scan time effect can be absorbed into the term for the angle κ of sensor exterior orientation.

COLLINEARITY EQUATIONS

Most photogrammetrists are familiar with the collinearity equations and their use with frame photography. A similar pair of equations may be derived for the recording of each resolution element using the geometric portion of the transformation in (6).

Writing the elements of $\underline{A}$ as a_{ij}, i = 1,2,3, j = 1,2,3, equation (22) may be written as

$$\begin{bmatrix} X - X_c \\ Y - Y_c \\ Z - Z_c \end{bmatrix} = \begin{bmatrix} a_{11} & a_{21} & a_{31} \\ a_{12} & a_{22} & a_{32} \\ a_{13} & a_{23} & a_{33} \end{bmatrix} \begin{bmatrix} 0 \\ (c/k)\ \tan\theta \\ -(c/k) \end{bmatrix}$$

Dividing the first and second equations by the third and rearranging

$$(X - X_c) = (Z - Z_c) \frac{a_{21}\tan\theta - a_{31}}{a_{23}\tan\theta - a_{33}}$$

$$= (Z - Z_c) \frac{a_{21}\sin\theta - a_{31}\cos\theta}{a_{23}\sin\theta - a_{33}\cos\theta} \tag{32a}$$

$$(Y - Y_c) = (Z - Z_c) \frac{a_{22}\tan\theta - a_{32}}{a_{23}\tan\theta - a_{33}}$$

$$= (Z - Z_c) \frac{a_{22}\sin\theta - a_{32}\cos\theta}{a_{23}\sin\theta - a_{33}\cos\theta} \tag{32b}$$

If $\underline{A}$ is taken equal to $\underline{I}$, $a_{ii} = 1$, and equations (32) reduce to the same results given in the section of idealized geometry. If six exterior orientation elements were assumed unknown for each scan, it would be impossible to have a

a solution and derive information from MSS data. Therefore, some type of functional behaviour (polynomials, etc.) must be assumed for these elements. Once decided, object space control may be used to determine the coefficients of these functions (resection), then equations (32) used to determine positions of other object points (intersection). The result would be a "rectified" data array. Obviously, all operations using equations (32) may be performed simultaneously.

EXPERIMENTAL RESEARCH

To incorporate the results of the analyses given above, a series of experimental steps were carried out in conjunction with LARS automated interpretive system. A description of these steps is given in the following subsections. One of the more important tasks is to assign elevations to each of the digital resolution elements. Therefore, the first subsection is devoted to the discussion of this operation.

Assignment of element elevation

Before any geometric corrections can be applied, an elevation Z_j must be assigned to each element of the data array. This is particularly necessary when the approximate procedures developed above are used. Element elevations may be derived from the MSS data itself if and only if the object is scanned more than once. Most present data pertain to singly scanned areas, and therefore elevations must be obtained from sources external to the MSS data. One such source, which was used for this investigation, is the topographic contour maps of the U.S. Geological Survey at a scale of 1:24000. The information may be gathered by digitizing X-Y coordinates along selected contour lines on a flat-bed coordinate digitizer. The coordinate information for the contours is recorded directly on punched card output. At the same time, the coordinates of selected ground control points may also be recorded. The digitized data thus obtained are then transformed to the MSS data using a similarity transformation, so that the remaining operations may be performed at the image scale.

At this point, a method must be found to reliably assign an appropriate elevation to every data array element. A seeming paradox exists, since the digitized contour information, although at image scale, is in an essentially orthographic projection, while the data arrays have all of the image displacements and distortions. The solution to the problem of superimposing the two data sets lies in the nature of the data itself. Since the data arrays can resolve only to the value, ΔY, given in equation (16), it is only necessary to be able to assign element elevations with an accuracy which will yield a planimetric error of this value of less after subsequent processing. Thus, by using ΔY of equation (16) is place of δY in equation (18), as an allowable planimetric error, and solving for the allowable height assignment error, the appropriate height assignment tolerance may be written as

$$\delta Z = \frac{\Delta Y}{\tan\theta} \quad (33)$$

$$Z = \frac{\gamma (Z_c - Z)}{\sin\theta \cos\theta} \quad (34)$$

Figure 7 shows graphically the magnitude of this allowable height assignment error, using equation (34). At nadir, the allowable error is infinite since a change in elevation has no effect on the image. The value of δZ decreases to a minimum at 45°, where planimetric error becomes equal to height assignment error. The allowable value then increases rapidly beyond 45°, since the ground size of a resolution element increases very rapidly beyond this point.

To superimpose the two data sets within this tolerance, it is necessary to find a transformation which will yield a height assignment error of less than that given in Figure 7. To do this, ground slopes must be considered.

In Figure 8, the term δY represents the planimetric error in superimposing the MSS digital arrays onto the digitized map information. The resulting elevation error is given by

$$\delta Z = \lambda \delta Y; \quad (35)$$

in which λ is the ground slope in the vicinity. If the allowable height assignment error from equation (33) is substituted into this expression and the resulting equation is solved for δY, then

$$\delta Y = \frac{\Delta Y}{\lambda \tan\theta} \quad (36)$$

which represents the allowable planimetric error which may be tolerated in an approximate transformation to relate data arrays and digitized map information for height assignment purposes, and still result in less than a one resolution element planimetric error after subsequent analysis. In reality, ground slopes rarely exceed 0.5, and scan angles (θ) normally do not exceed 40°. Thus a transformation yielding errors on the order of 3 resolution elements may be appropriate for this step of height assignment. The affine transformation proved adequate for this purpose.

The digital data arrays are processed through the affine transformation, to bring them as close as possible to the scaled digitized map data. Each digitized contour is then traced digitally using a computer program, and all intersections of this contour with each transformed scan line are found. All contour-scan intersections are thus located for every scan line down the strip. Points along the scans intermediate between these intersection points may be assigned elevations by linear interpolation.

It should be noted that the affine transformation is used only for elevation assignments. The spectral values within the data arrays are left unaltered, and the element positions remain the same before and after element height

assignments. That is, the image element positions are restored to their original distorted positions after the assignment of elevations, in order that the more refined geometric techniques using polynomials or collinearity equations may be utilized.

All of the above is predicated upon the fact that only singly scanned imagery is available. If overlapping imagery is available, then it may be possible to compute element elevations from the MSS data itself by forming intersections. Several investigators (4,8,11) have addressed this problem within the context of model formation and relative orientation. Since only singly scanned imagery was available for this investigation, this approach has not been considered.

Application of approximate polynomials

We have shown previously that polynomials such as those of equations (29) and (30), or similar others, can be derived to approximate the effects of sensor exterior orientation elements. To apply these polynomials, it is important that scan angle and topographic effects are accounted for first. If the data is acquired over flat terrain, where there is no effect due to topography, the polynomials may be used directly since they account for the scan angle through the series expansion of $\tan\theta$, etc. This is particularly appropriate when the scan angles are small. On the other hand, when relief exists and the scan angles are not small an alternative method derived for use with LARS programs (17), may be used.

The procedure consists of resampling along each scan line such that every sample elements represents an equal Y - interval on the datum instead of equal angle at sensor. Consequently, the total number of elements in each sample line remains the same as before resampling. Figure 10 illustrates the geometric basis for the resampling algorithm in which:

- n is the number of samples from beginning of scan to nadir
- N is the total number of sample elements in each scan line
- S_i is the spectral value in the ith element before resampling
- S_i' is the spectral value in the ith element after resampling
- d_i is the distance from the scan edge to the center of the ith element
- W is the total width (along datum) of ground coverage
- h_1, h_N are the flying heights above the first and last elements.
- Δh_i is the elevation difference between the ith and first sample points

The algorithm seeks to find a variable sample angle, $U_i\ \gamma$, for every element, such that the resampled data represents elements of equal length on the datum.

The multiplier, U_i, may be considered as having an integer portion, L_i, and a fractional portion, C_i, and may thus be written as

$$U_i = L_i + C_i \tag{37}$$

The resampling multiplier, U_i, may be shown to be given by the expression (14,17)

$$U_i = \frac{1}{\gamma}\left\{n\gamma + \tan^{-1}\left[\frac{1}{h_1 - \Delta h_i}\left(\frac{2i-1}{2N} h_N \tan(N\gamma - n\gamma) + \frac{2i-1}{2N} \tan n\gamma - h_1 \tan n\gamma\right)\right]\right\} \tag{38}$$

This expression is computed for each element in every scan line. The spectral value stored in the ith resampled element may be computed by interpolation of spectral values from the original array. If linear interpolation is applied the result is

$$S_i' = S_{L_i} + C_i \left(S_{L_i+1} - S_{L_i}\right) \tag{39}$$

Figure 9 displays the effect of resampling on the position of sample points for a real data case. The solid line represents an algorithm for flat terrain, while the dotted line takes terrain relief (approximately 150 feet) into account. Note that sample points at the beginning, middle, and end of a scan line are displaced very little, while those in between experience displacements of as much as 7 or 8 elements.

Once resampling is accomplished, polynomials may then be used to determine horizontal positions (X, Y) of desired points, from given control. Preliminary experience indicate that this approximate technique is applicable only to relatively flat areas.

A danger in the use of this method lies in the fact that interpolation of spectral values is done during resampling. This increases the possiblity that the automated interpretation algorithms may achieve a lower accuracy of classification.

Application of collinearity equations

The collinearity equations of (32a) and (32b) may be applied directly to the digital data. Since all our activities for this investigation so far have been concerned with simple imagery, elevations of all terrain points of interest must be known a priori, as has been discussed previously. In order to apply equations (32), some functional form for each of the pertinent elements of sensor exterior orientation must be assumed. Once this is done, a rigorous adjustment program may be set up to determine the required planimetric coordinates in one simultaneous solution. The end result would be a rectified data arrays referring to an orthographic system, where each element is designated by all three ground coordinates, and contains as many spectral values as the number of scanner channels.

To demonstrate the application of the collinearity equations to geometric analysis of MSS data arrays, two flight lines of real data were chosen for analysis. Both were flown during the corn blight watch experiment administered by LARS during the summer of 1971. The first of these, flight no. 208, was located in northwestern Indiana, near the city of Lafayette. Terrain variation within the flight line is quite small, on the order of 50 feet over the entire flight line. A large percentage of the ground was under cultivation, with no forest cover. A grey scale computer printout of the data arrays for the flight line was generated, from which intersection of roads, fences and streams recognizable both on the display and the map were chosen as control points. The area contains many section roads and fence lines, with well defined, nearly perpendicular, intersections. Reliability in assignment of line-column positions on the grey scale display for the control points was on the order of one or two resolution elements.

The second flight line chosen, flight no. 218, is located in west central Indiana, near the city of Bloomington. Total terrain variation within the flight line is on the order of 300 feet. Most of the area is wooded such that a tree canopy obscures much of the ground. Greater difficulty was encountered in the determination of array positions from the grey scale display for control points with this flight line. Uncertainties in array location assignments of 3 to 4 resolution elements were not unusual.

For each of the flight lines two analyses were carried out. In the first case, one set of functions for the pertinent sensor exterior orientation elements was assumed for the entire length of the flight line. The positional elements X_c, Y_c, were assumed as second order polynomials. The flying height, Z_c, and the angle κ, were assumed constant down the flight line. Since the scanner used was stabilized in ω, the term was taken as zero. The ϕ term was also taken as zero, due to its high correlation with X_c.

In the second case, the same assumptions were made for the functional forms of the sensor exterior orientation elements, but the flight line was broken into sections, each section having its own functional parameters.

Tables I and II summarize the results obtained for flight no. 208. The residuals given are in terms of resolution elements at image scale. From Table I, treating the entire flight line as a unit, the reference variance obtained, $\hat{\sigma}_o^2$, was 1.73 with 68 degrees of freedom. In Table II, treating the data in five sections a pooled reference variance of 0.88 was obtained, with 54 degrees of freedom. An F test of these variances indicates a significant improvement at the 95% level in treating the data in sections.

TABLE I

Residuals for Flight No. 208, Treating Entire Flight Line as a Unit

CONTROL POINT	RESIDUALS X	Y
1	-1.50	-1.40
2	1.84	-0.40
3	2.71	-0.28
4	0.93	1.24
5	1.25	0.30
6	-2.82	-2.26
7	0.22	0.64
8	-1.72	2.87
9	*	*
10	-1.32	1.47
11	-0.77	0.60
12	0.46	-0.70
13	-0.91	0.20
14	1.44	-0.04
15	-1.15	-0.02
16	-1.50	0.01
17	-1.17	-0.88
18	2.14	0.30
19	2.36	1.00
20	2.03	-0.16
21	0.92	-0.59
22	0.50	-1.33
23	0.13	-0.61
24	-0.34	-0.61
25	-1.08	-0.25
26	-0.20	0.94
27	-0.85	0.37
28	-0.13	-0.37
29	-0.77	0.22
30	-0.23	0.83
31	-0.98	-0.29
32	-2.14	-0.22
33	-1.39	-1.92
34	0.74	-0.62
35	0.65	-3.12
36	1.03	0.55
37	1.88	1.06
38	-1.03	2.15
39	0.77	0.83

$\hat{\sigma}_o^2 = 1.73$, $\hat{\sigma}_o = 1.31$, d.f. = 68

* Data point rejected due to data blunder

TABLE II

Residuals for Flight No. 208, Treating Entire Flight Line in Sections

CONTROL POINT	BLOCK NUMBER	RESIDUALS X	RESIDUALS Y	X	Y
1		0.42	0.43		
2		0.03	-0.34		
3		0.65	-0.69		
4	I	-0.70	0.86		
5	$\hat{\sigma}_o^2$ = 0.47	0.07	-0.11		
6	$\hat{\sigma}_o$ = 0.69	-0.40	-0.39		
7	d.f. = 10	-0.07	0.26		
8		-0.60	0.70	0.10	0.52
9		*	*	*	*
10		0.60	-0.72	-0.10	-0.11
11				-0.04	-0.59
12	II			-0.05	-0.34
13	$\hat{\sigma}_o^2$ = 0.45			-0.37	-0.12
14	$\hat{\sigma}_o$ = 0.67			1.35	0.44
15	d.f. = 10			-1.06	0.57
16				0.26	-0.14
17		-1.57	-0.04	-0.08	-0.28
18		-1.69	-0.89		
19		1.59	0.47		
20	III	1.89	1.13		
21	$\hat{\sigma}_o^2$ = 1.76	1.11	-0.01		
22	$\hat{\sigma}_o$ = 1.32	-0.45	-0.42		
23	d.f. = 10	0.58	-0.58	0.50	-0.41
24		-0.26	0.15	0.13	0.19
25		-1.19	0.18	-0.34	0.07
26	IV			-0.72	0.37
27	$\hat{\sigma}_o^2$ = 0.29			0.36	0.60
28	$\hat{\sigma}_o$ = 0.54			-0.28	-0.03
29	d.f. = 10	-0.28	-0.12	0.44	-0.83
30		-0.39	-0.32	-0.32	-0.15
31		-0.18	1.07	0.24	0.20
32		-1.47	1.32		
33	V $\hat{\sigma}_o^2$ = 1.28	-0.64	-0.77		
34	$\hat{\sigma}_o$ = 1.13	1.56	0.12		
35	d.f. = 14	0.99	-1.85		
36		0.21	-0.11		
37		0.98	0.25		
38		-1.64	0.80		
39		0.08	-0.39		

Pooled $\hat{\sigma}_o^2$ = 0.88, pooled $\hat{\sigma}_o$ = 0.94, pooled d.f. = 54

Table III summarizes the results obtained in treating flight no. 218 as a unit. A reference variance of 6.03 was obtained, with 56 degrees of freedom. In Table IV, treating the data in four sections, a pooled reference variance of the 3.46, with 38 degrees of freedom was obtained. An F test once again revealed a significant difference at the 95% level, between the two methods of analysis.

Figure 11 depicts a visual grey scale representation of the data arrays for flight no. 208. Figure 11a shows the data before any geometric treatment, and figure 11b shows the results of treatment using collinearity equations in five sections down the strip. Figure 12a depicts the uncorrected imagery for flight no. 218, and figure 12b illustrates the results after treatment using the collinearity formulation in four sections.

Flow chart of MSS system analysis

The following chart summarizes the system which has been presented in this paper for the geometric analysis of MSS digital Arrays.

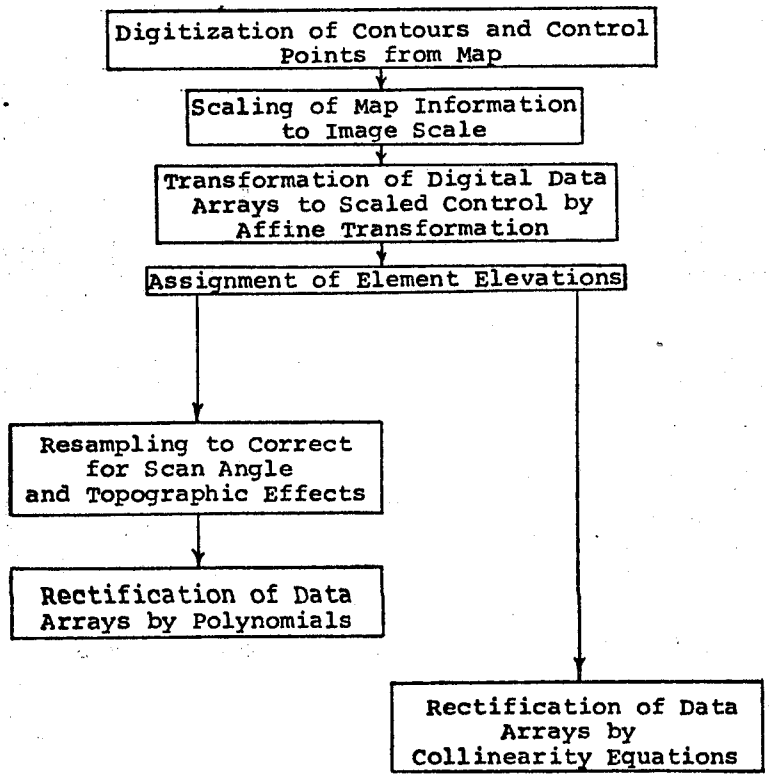

TABLE III

Residuals for Flight No. 218, Treating Entire Flight Line as a Unit.

CONTROL POINT	RESIDUALS X	Y
1	2.46	2.84
2	-3.42	-0.24
3	3.24	-1.79
4	2.77	2.69
5	-2.57	0.60
6	-4.71	1.38
7	-3.35	0.30
8	1.98	-0.19
9	-0.26	-2.84
10	-0.34	-1.41
11	3.35	-2.78
12	1.68	-2.26
13	0.72	-1.97
14	-3.60	-0.02
15	-2.10	-0.06
16	0.69	-2.72
17	2.69	0.48
18	-0.19	-0.30
19	5.65	-1.83
20	-1.91	1.46
21	1.01	2.75
22	1.30	1.56
23	-1.07	1.15
24	-1.94	4.37
25	-1.71	2.29
26	*	*
27	-1.24	3.59
28	-2.27	2.20
29	2.12	0.24
30	-2.36	-2.53
31	3.57	-1.66
32	0.89	-3.53
33	0.23	-1.74

$\hat{\sigma}_o^2 = 6.03$, $\hat{\sigma}_o = 2.46$, d.f. = 56

TABLE IV

Residuals for Flight No. 218, Treating Flight Line in Sections

CONTROL POINT	BLOCK NUMBER	RESIDUALS X	RESIDUALS Y	X	Y
1		1.59	0.48		
2	I	-4.50	-1.16		
3	$\hat{\sigma}_o^2$ = 8.38	1.66	0.25		
4	$\hat{\sigma}_o$ = 2.89	2.48	0.61		
5	d.f. = 6	-0.26	-0.89		
6		-2.26	0.73		
7		1.29	-0.04	0.04	-0.19
8				-0.61	1.56
9	II			0.58	-0.84
10	$\hat{\sigma}_o^2$ = 0.81			-0.31	0.56
11	$\hat{\sigma}_o$ = 0.89			0.17	-0.96
12	d.f. = 10			0.11	-0.37
13				0.49	-0.31
14				-0.84	0.82
15		-0.35	-0.69	0.37	-0.27
16		-1.22	-0.59		
17	III	2.59	1.23		
18	$\hat{\sigma}_o^2$ = 3.87	-1.61	0.83		
19	$\hat{\sigma}_o$ = 1.97	2.19	-1.05		
20	d.f. = 10	-2.38	-0.36		
21		1.07	0.86		
22		1.73	-0.48		
23		-2.02	0.27	-0.16	-0.83
24				-0.59	1.91
25				1.86	-1.17
26				*	*
27	IV			-0.01	0.95
28	$\hat{\sigma}_o^2$ = 2.87			-1.09	-0.06
29	$\hat{\sigma}_o$ = 1.70			-2.21	0.22
30	d.f. = 12			0.09	-2.04
31				2.61	0.30
32				-1.55	0.02
33				1.04	0.71

Pooled $\hat{\sigma}_o^2$ = 3.46, pooled $\hat{\sigma}_o$ = 1.86, pooled d.f. = 38

CONCLUSIONS

This paper was begun by a very brief survey of remote sensing systems in order to show how the MSS system under consideration is categorized. Because of the extensive amount of data acquired by the MSS, an automated digital technique based on pattern recognition and statistical classification algorithms has been developed by, and is used at, LARS of Purdue. Because, at the time the system was developed, the geometric factors of the sensor were subordinated to those of interpretive interest, it became apparent recently that an analysis of these factors would enhance the value of the acquired data.

Instead of discussing the geometric factors of MSS as a separate and isolated problem, a philosophy was advanced at the beginning of this paper in which remote sensing in general is regarded as a mapping or transformation. This transformation should ideally operate on all variables involved, both metric and non-metric. Because of the specified purpose of the paper, we limited consideration to the four dimensions of geometric space and time. The development proceeded to deal with specialized cases and approximations -- all of which were shown to be included in the general transformation. The specializations were dictated by the fact that the research is being performed within the bounds of an already existing digital classification algorithm. The adoption of this course of action was mainly for reasons of expediency since it made possible the attainment of some results, as given in the text.

Ideally, one should strive to work with the unified concept. In addition to the metric variables considered, non-metric factors arising from the broad subject of interaction between radiation and matter should also be taken into account in the transformation. Consequently, the object space vector may be enlarged to include: spectral radiance from each resolution element at a particular wavelength; polarization of the radiant energy with respect to the object space coordinate system; and the coherence, both spatial and temporal, of the radiant waves. Likewise, the sensor space vector may be expanded to include, spectral irradiance incident on the sensor corresponding to each resolution element at a particular wavelength; polarization as to whether retained or not, and if retained its direction with respect to the sensor coordinate system; coherence, whether partially or totally lost; and frequency and phase shifts which are useful when active remote sensing systems are utilized.

The ultimate in treating remote sensing systems is to seek as general a transformation as possible, that is, one which can be applied to any system. Such a transformation would include all elements involved, both metric and non-metric, and may be used both for interpretive as well as for quantitative purposes. The development of this concept is obviously well beyond the scope of this paper. However, it is felt that the unified idea advanced here merits serious consideration and research is in fact continuing on its development.

ACKNOWLEDGEMENTS

The authors wish to recognize the role of the Laboratory for the Applications of Remote Sensing (LARS) of Purdue University in making this research possible through the use of their programs. Special thanks are due Mr. Paul Anuta of the Laboratory for his generous assistance in regard to the use and modifications of the programs. The authors would like also to acknowledge contributions by Dr. John C. Trinder, of the University of New South Wales, Australia, who, while on sabbatical leave at Purdue, worked on the early phase of the research with one of the authors.

Thanks are also due Mr. S. A. Hempenius of the International Institute for Aerial Survey and Earth Sciences (ITC), the Netherlands, for extensive discussions with the other author during the latter's sabbatical at ITC. It was through these discussions that the author was able to formulate the unified concept mentioned in the paper.

The authors also express their appreciation to Dr. G. W. Marks for reviewing portions of the text, Mr. R. A. Gordon for assisting in preparing the figures, and Mrs. Jo Anne Gray and Miss Molly Wood, for getting the paper typed within the limited time made available to them by the authors.

BIBLIOGRAPHY

1. Anuta, P., "OVERLA", unpublished program and documentation written for L.A.R.S.

2. Case, J. B., "The Analytic Reduction of Panoramic and Strip Photography", Photogrammetria, 1967.

3. Committee on Remote Sensing for Agricultural Purposes, National Research Council", Reomote Sensing with Special Reference to Agriculture and Forestry", National Academy of Sciences, Washington, D.C., 1970.

4. Derenyi, E., "An Exploratory Investigation Concerning the Relative Orientation of Continuous Strip Imagery", Tech. Report #8, Department of Surveying Engineering, University of New Brunswick, Fredricton, N.B., Canada, 1971.

5. Derenyi, E. and Konecny, G., "Geometry of Infrared Imagery", Canadian Surveyor, Volume XVIII, No. 5, 1964.

6. Derenyi, E. and Konecny, G., "Infrared Scan Geometry", Photogrammetric Engineering, Volume XXXII, No. 5, September 1966.

7. Knight, C., "Computer Generated Displays of Terrain from Digital Terrain Data", paper presented at A.S.P. Spring convention, March, 1972.

8. Konecny, G., "Geometrical Aspects of Remote Sensing", paper presented to Commission IV, Twelfth International Congress of Photogrammetry, Internation Society of Photogrammetry, Ottawa, Canada, 1972.

9. Kratky, V., "Precision Processing of ERTS Imagery", presented at the fall meeting, A.S.P., September 1971.

10. Kraus, K. and Mikhail, E. M., "Linear Least Squares Interpolation", presented at the Twelfth Congress of the International Society of Photogrammetry, Ottawa, Canada, 1972.

11. Leberl, F., "Untersuchung uber die Geometric und Einzelbildauswertung von Radarschraganfnahmen", Dissertation, Technical University Vienna, 1971.

12. Leberl, F., "Metric Properties of Imagery Produced by Side-Looking Airborne Radar and Infrared Linescan Systems", Proceedings of the ISP Commission IV Symposium", ITC series A, No. 50, 1971.

13. Leberl, F., "Vorschlage zur instramentellen Entgerrung von Abbildungen mit Seitwarts-Radar (SLAR) und Infrarotabtastsystemen (IRLS), B.M.L., 1971/2.

14. Phillips, T., "EQUDST", unpublished program and documentation written at L.A.R.S.

15. Shepard, W., "Automatic Contour Digitizer", Photogrammetric Engineering, January, 1968.

16. Taylor, J., "Rectification Equations for Infrared Line-Scan Imagery", Commission IV Symposium, ITC series A, No. 50, 1971.

17. Trinder, J., "EQUDST, a Generalization", unpublished document written at LARS.

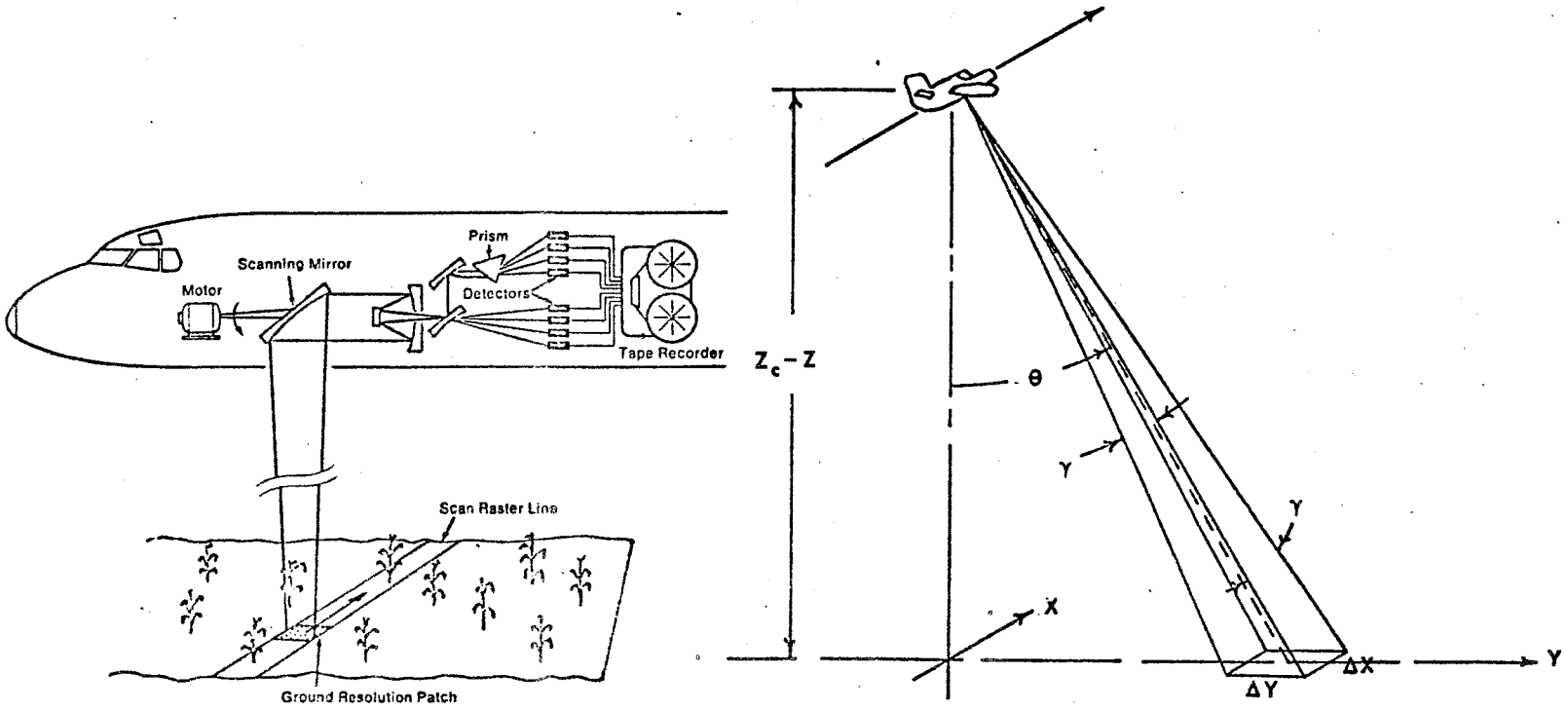
Prism
Scanning Mirror
Motor
Detectors
Tape Recorder
Scan Raster Line
Ground Resolution Patch
$Z_c - Z$
θ
γ
γ
γ
X
Y
ΔX
ΔY

a. b.

FIGURE 1

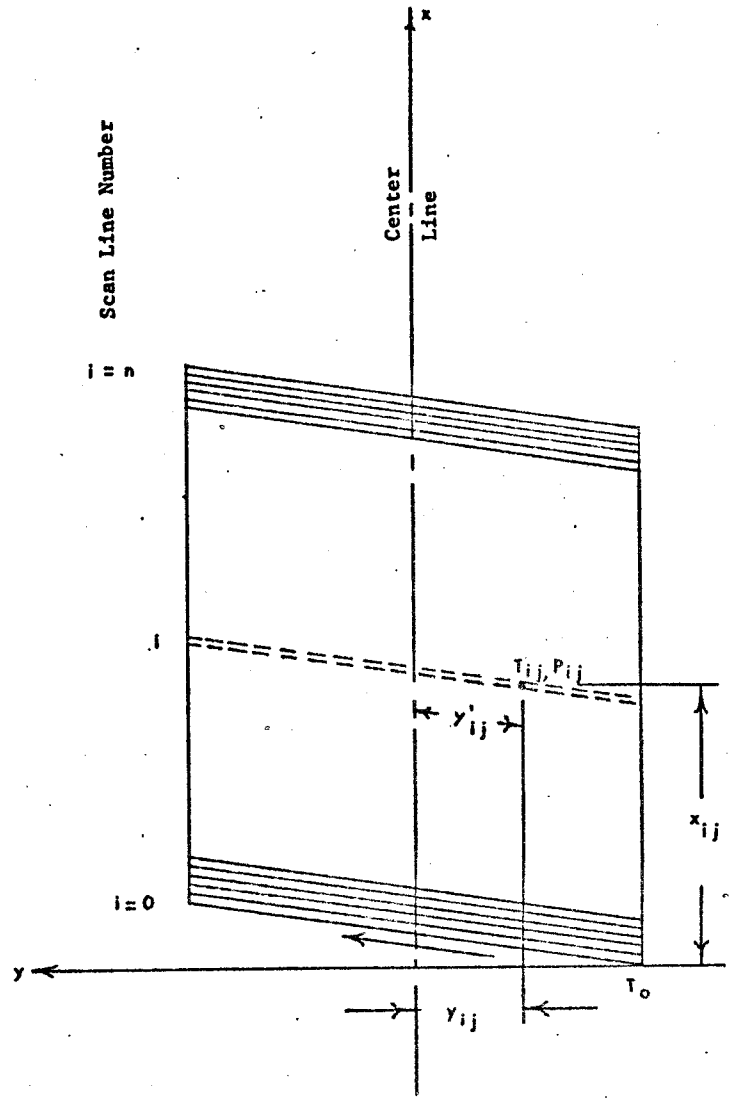

FIGURE 2

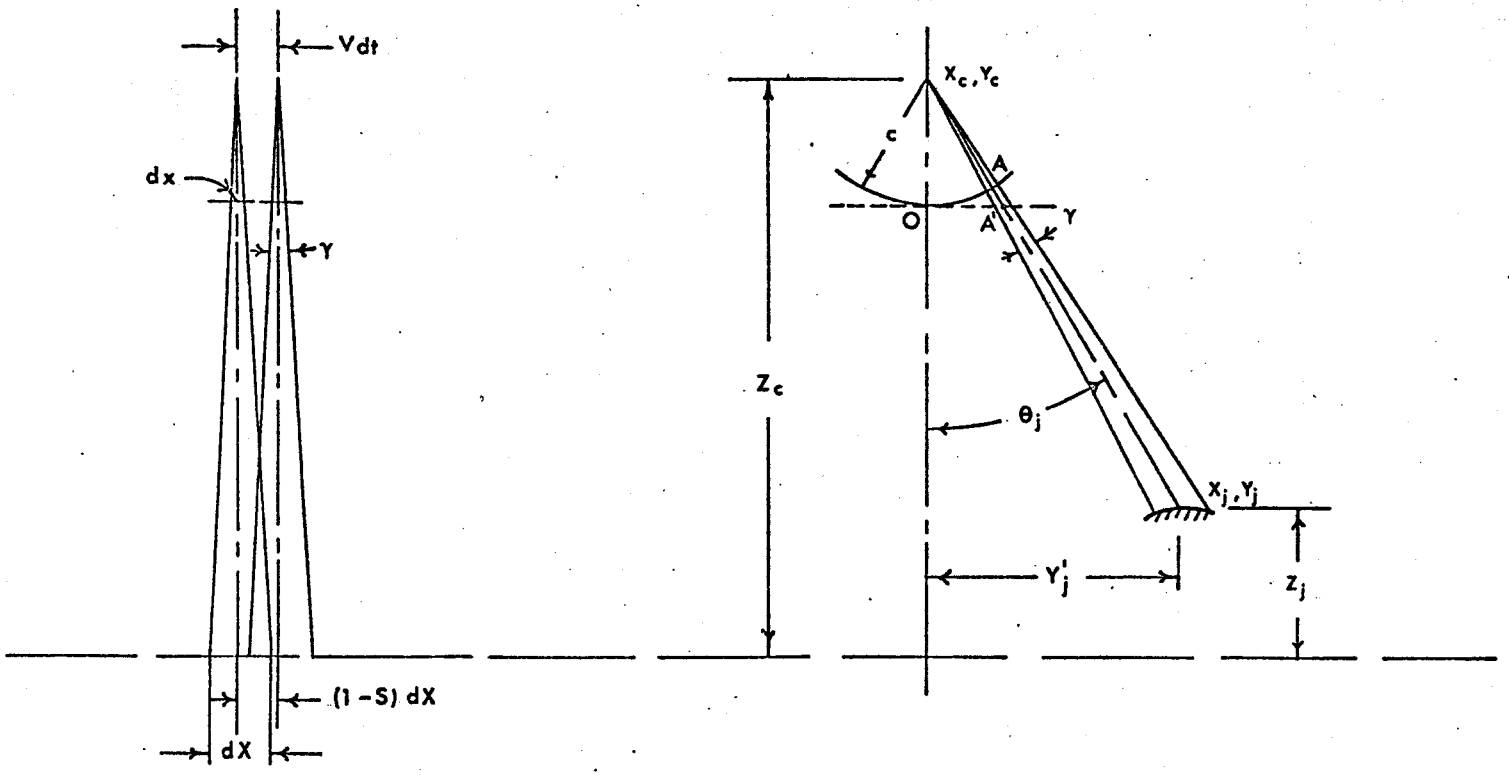

FIGURE 3

FIGURE 4

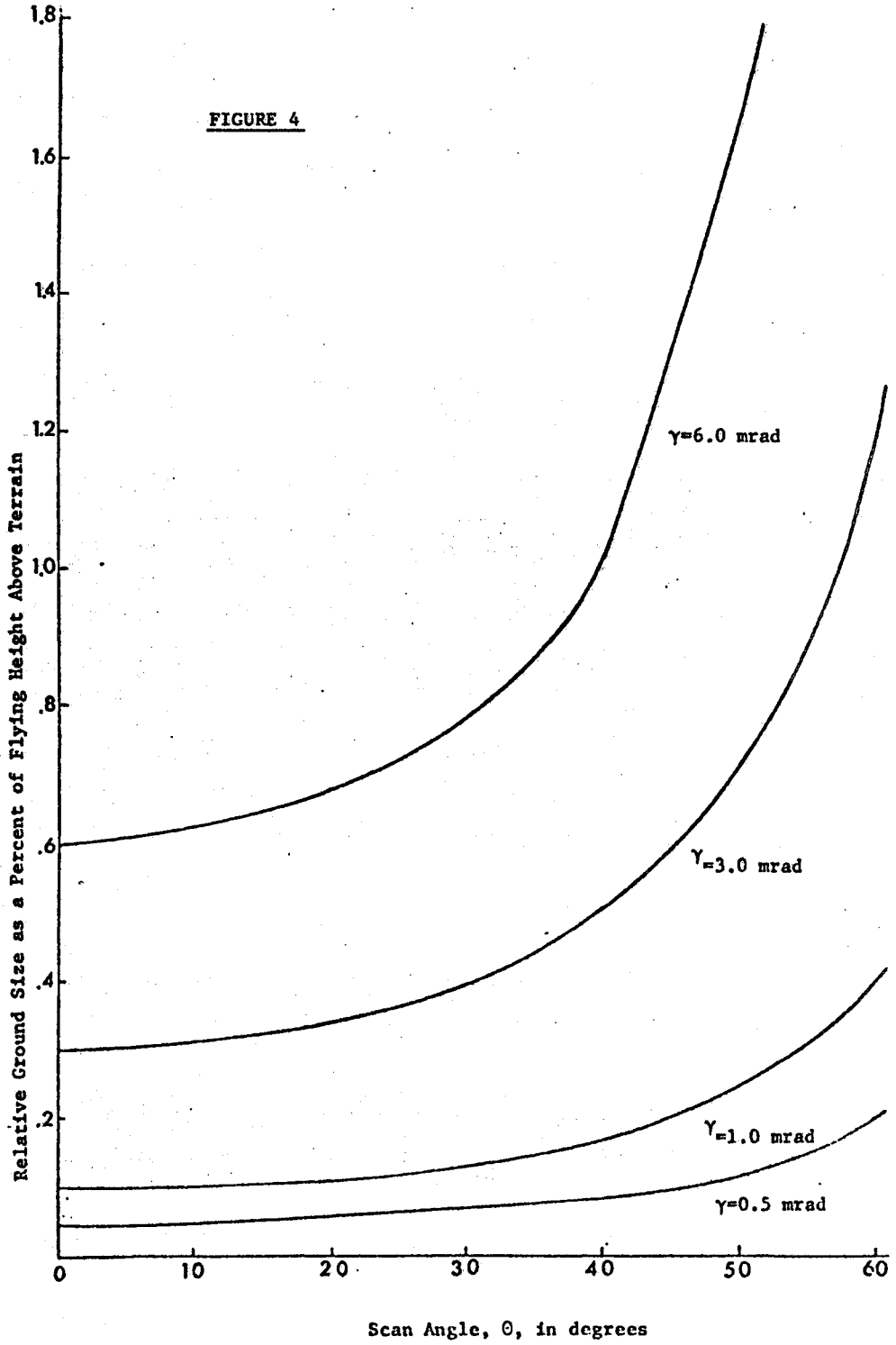
Relative Ground Size as a Percent of Flying Height Above Terrain
1.8
1.6
1.4
1.2
1.0
.8
.6
.4
.2
0
10
20
30
40
50
60
γ=6.0 mrad
γ=3.0 mrad
γ=1.0 mrad
γ=0.5 mrad
Scan Angle, θ, in degrees

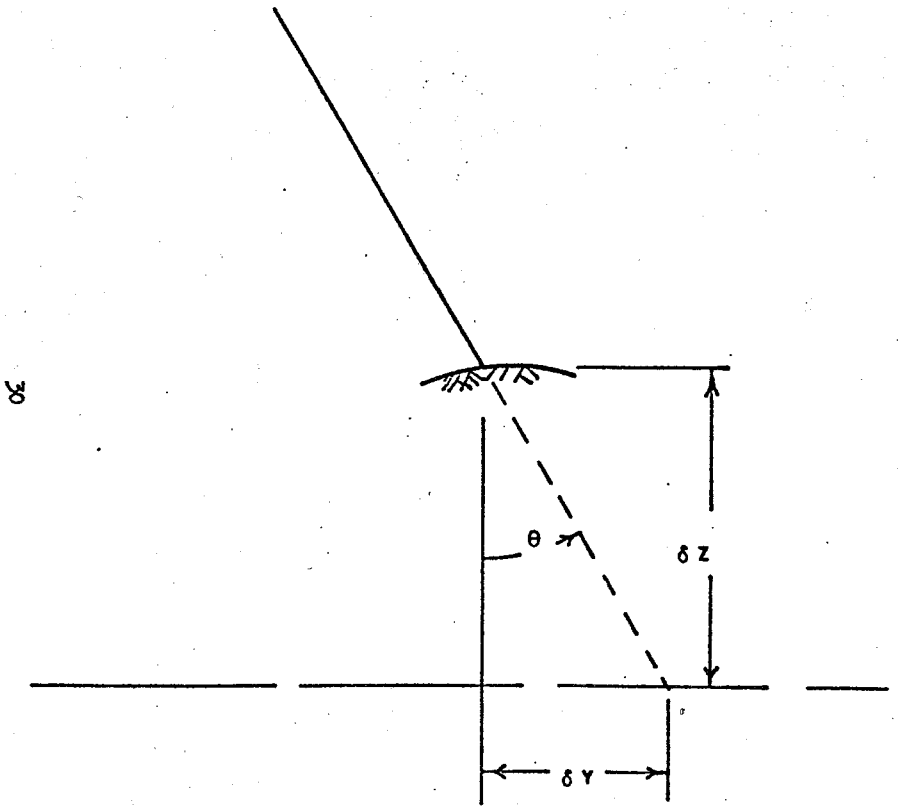

FIGURE 5

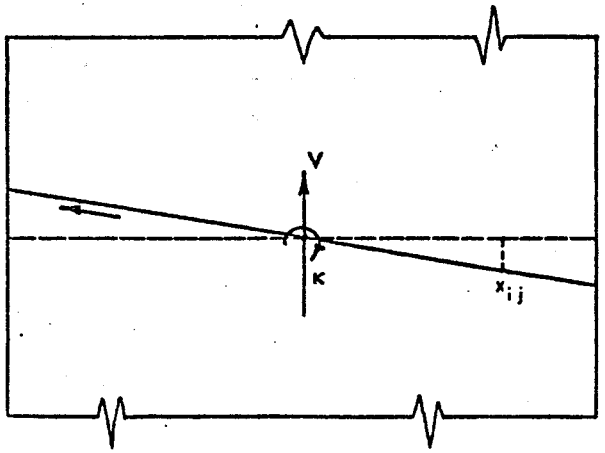

FIGURE 6

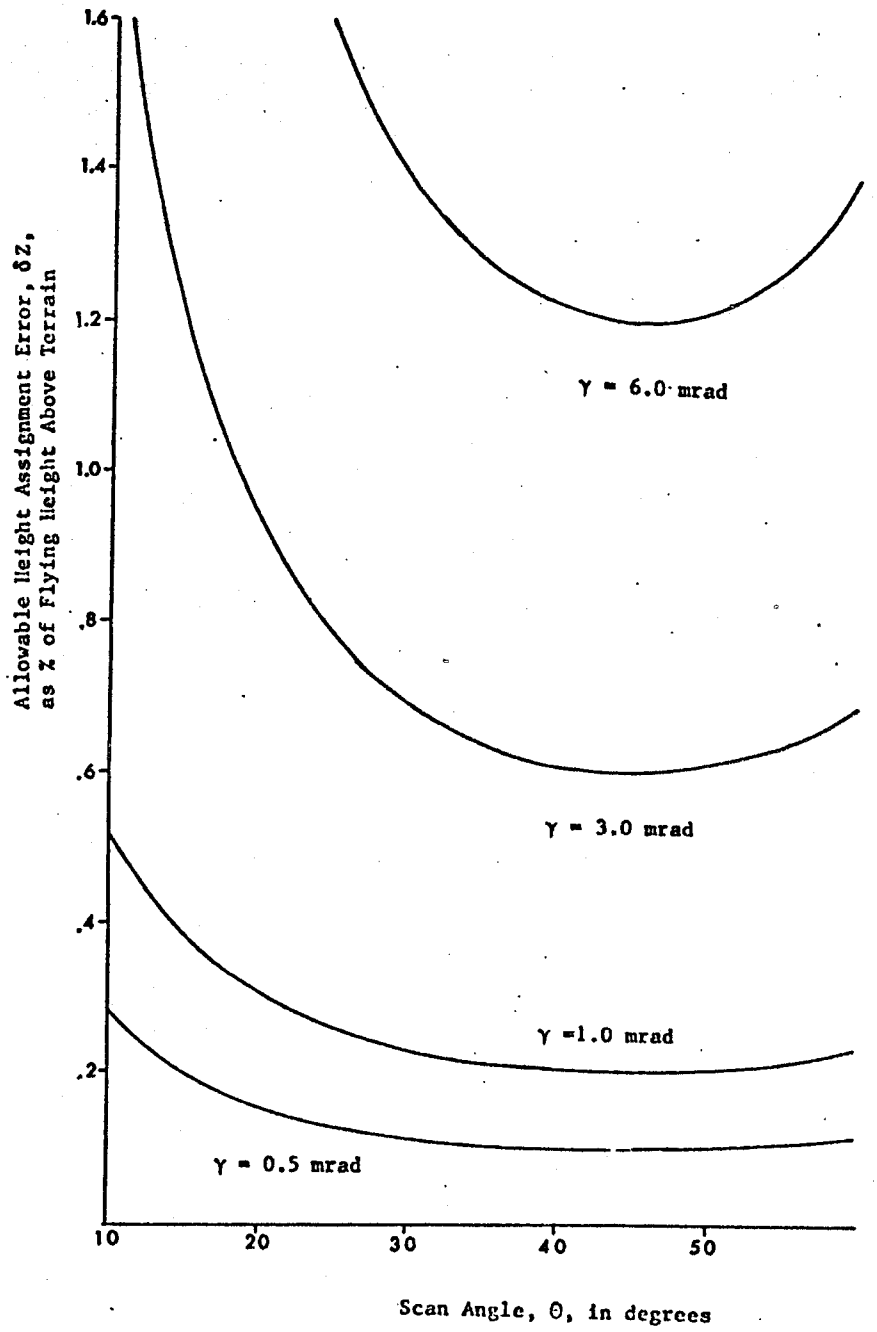
Allowable Height Assignment Error, δZ,
as % of Flying Height Above Terrain
1.6
1.4
1.2
1.0
.8
.6
.4
.2
γ = 6.0 mrad
γ = 3.0 mrad
γ =1.0 mrad
γ = 0.5 mrad
10
20
30
40
50
Scan Angle, θ, in degrees

FIGURE 7

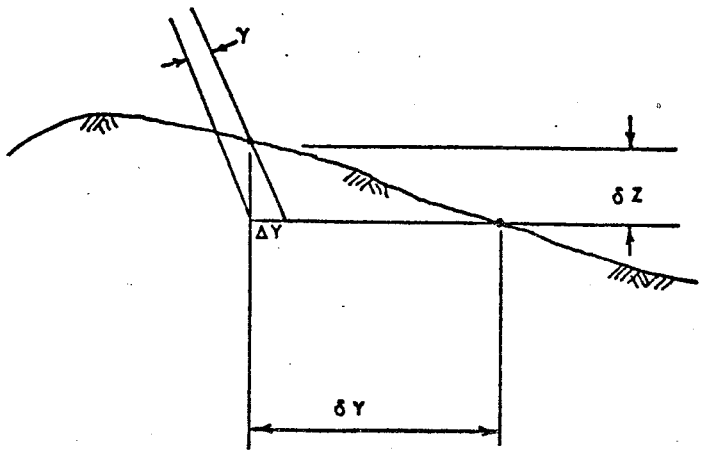

FIGURE 8

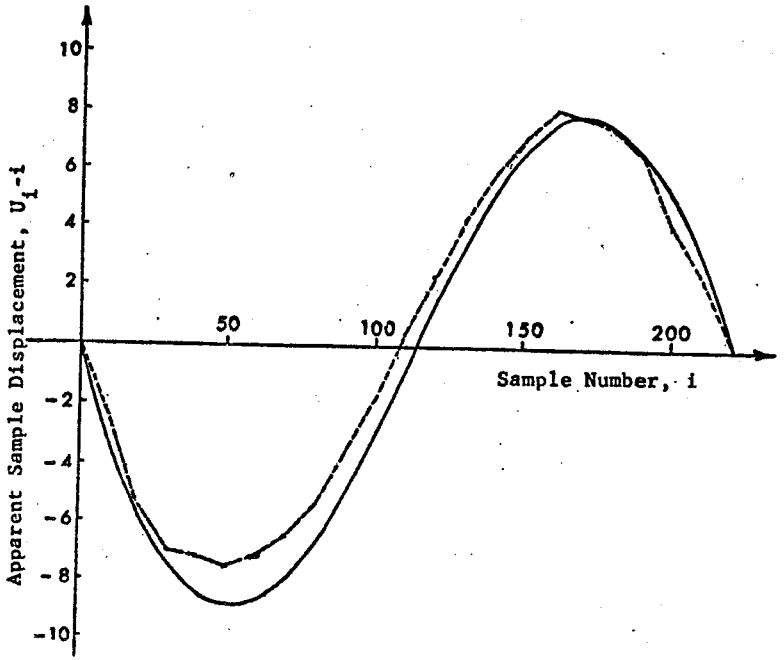

FIGURE 9

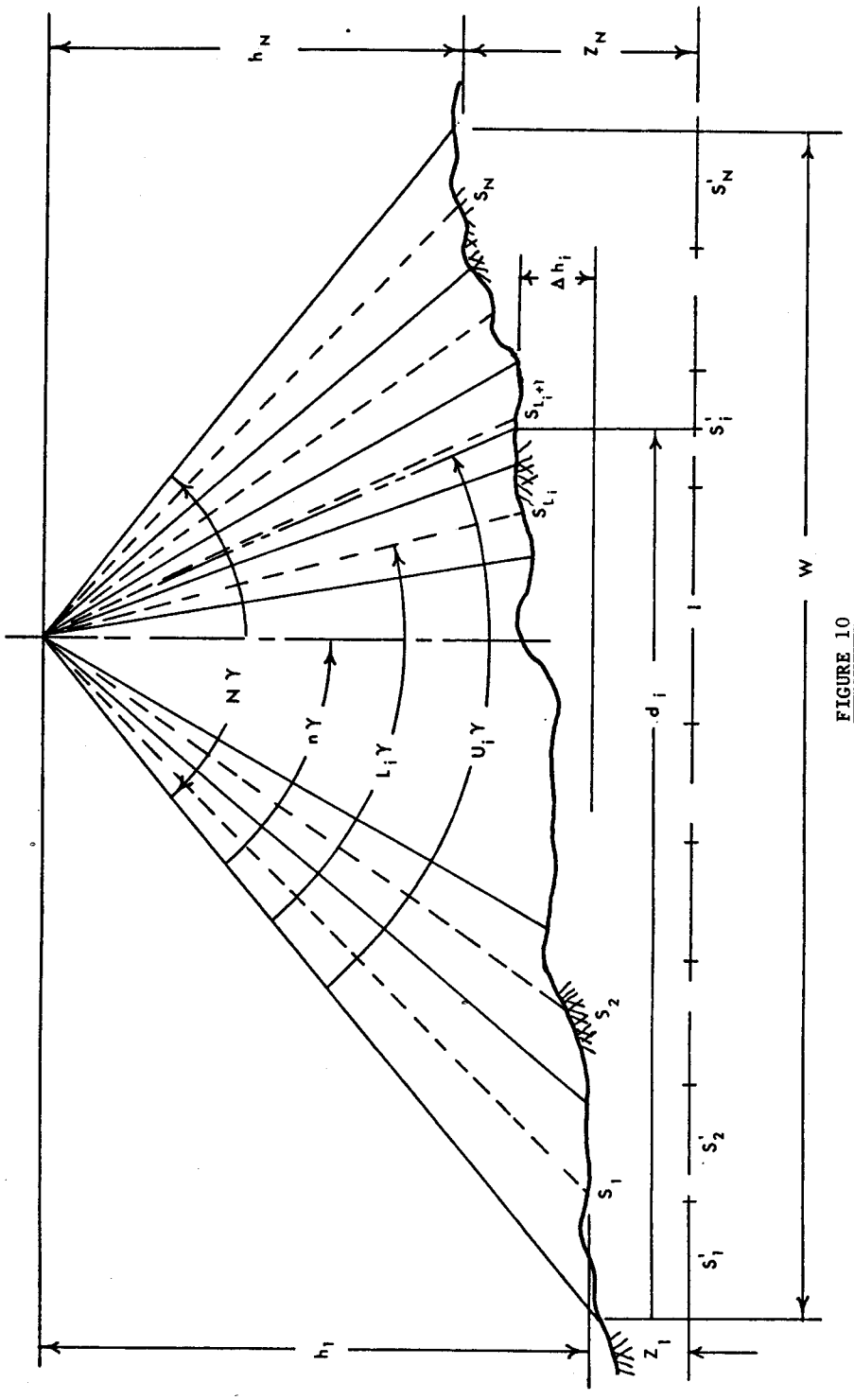
h_N
Z_N
S_N
S'_N
Δh_i
S_{L_i+1}
S'_i
S_{L_i}
N Y
$_nY$
L_iY
U_iY
d_i
I
W
S_2
S_1
S'_2
S'_i
h_1
Z_1

FIGURE 10

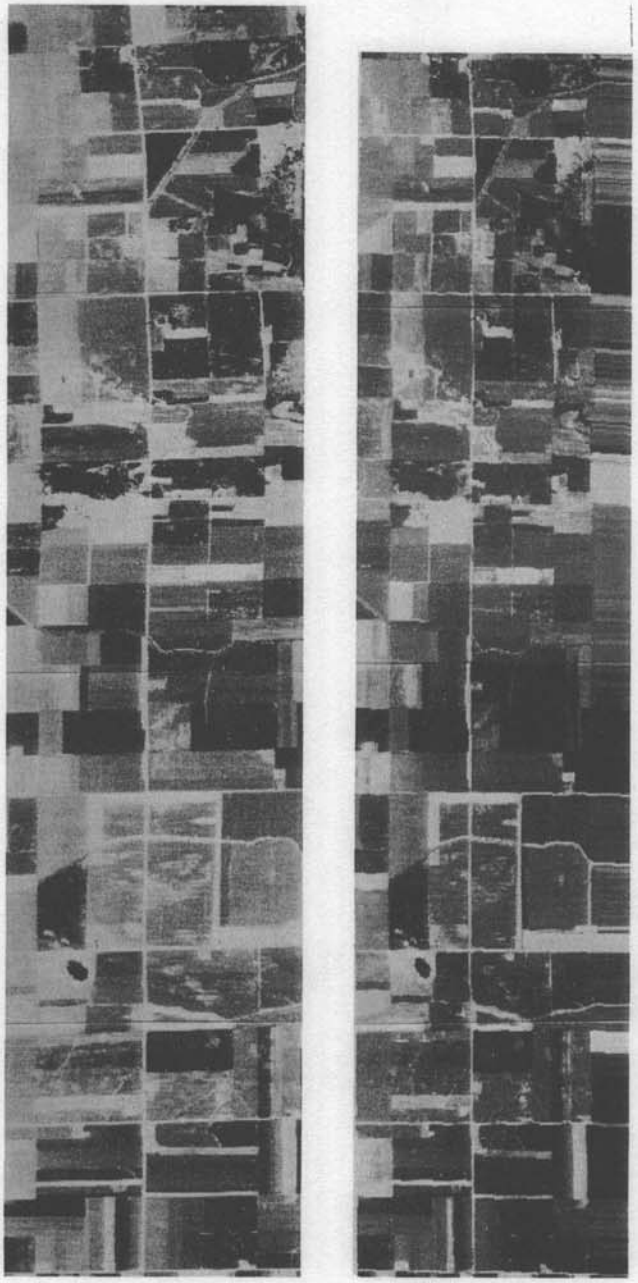

a. b.

FIGURE 11

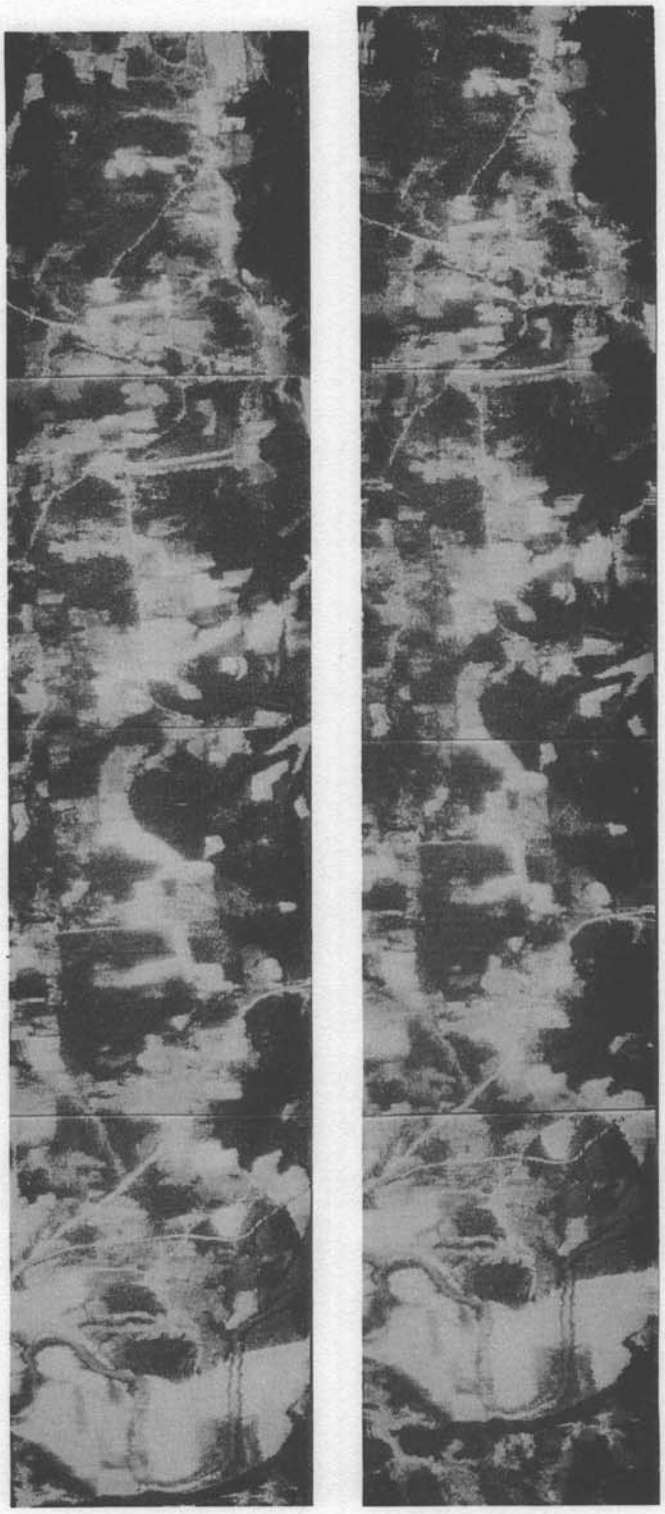

a. b.

FIGURE 12